Research Article Vol. 59, No. 5 / 10 February 2020 / Applied Optics A123

applied optics

Broadband phase-shifting mirrors for ultrafast lasers

M. Trubetskov,[1] T. Amotchkina,[2,*] L. Lehnert,[1] J. Sancho-Parramon,[3] K. Golyari,[1] V. Janicki,[3] M. Ossiander,[1] M. Schultze,[2] and V. Pervak[2]

[1]Max-Planck-Institut für Quantenoptik, Hans-Kopfermann-Str. 1, 85748 Garching, Germany
[2]Ludwig-Maximilians-Universität München, Am Coulombwall 1, 85748 Garching, Germany
[3]Ruder Boškovic Institute, BijenickaCesta 54, 10002, Zagreb, Croatia
*Corresponding author: Tatiana.Amotchkina@physik.uni-muenchen.de

Received 12 September 2019; accepted 19 November 2019; posted 22 November 2019 (Doc. ID 377746); published 20 December 2019

Metal–dielectric phase-shifting multilayer optical elements have been developed, providing broadband, virtually dispersion-free polarization manipulation down to the few-cycle level. These optical elements are Ag/Al_2O_3 mirrors that operate in the spectral range from 500 to 100 nm, exhibiting reflectance higher than 95%, and a differential phase shift between the s- and p-polarization of about 90° distributed over four bounces. The mirrors have been designed, produced, and reliably characterized based on spectral photometric and ellipsometric data using a non-parametric approach as well as a multi-oscillator model. The optical elements were implemented into a few-cycle laser system, where they transformed linearly polarized few-cycle light pulses to circular polarization.

https://doi.org/10.1364/AO.59.00A123

1. INTRODUCTION

Although metal–dielectric coatings are well known and have been widely used for many years, interest in them is constantly growing. Metal–dielectric coatings can be used as high reflectors, absorbers, cutoff filters, and color optical elements (see, for example, Refs. [1,2]). Recently, a few more interesting applications have been reported, including their use in solar cells [3–5]. In Ref. [6], metal–dielectric broadband absorbers were designed. Bicolor coatings containing metal-island films were reported in Ref. [7]. Metal–dielectric coatings are also in high demand for ultrafast laser applications. Ref. [8] reported the design and fabrication of optical coatings separating the radiation of CO_2 and He–Ne lasers. Metal–dielectric multilayers have been also actively investigated as novel photonic structures such as hyperbolic metamaterials [9] or epsilon near-zero media [10].

In order to design and produce metal–dielectric multilayers, one must know accurately the optical parameters of metal films. The complex refractive index of metals in the optical range is determined by several light–matter interaction processes such as interband and intraband transitions, and there has been continuous effort to establish dispersion models able to provide an accurate description of these phenomena [11,12]. In Refs. [13,14], a non-parametric approach for reliable characterization of thin metal films is presented. The results provided by the approach are very close to the optical constants delivered by the multi-oscillator model [14].

In the present work, a new laser application of metal–dielectric coatings is developed. By carefully tuning the thickness of the dielectric overcoating, a broad-band phase-shifting metal–dielectric mirror [15] for visible light is demonstrated. Unlike the currently available achromatic wave plates, which consist of multiple transmissive birefringent plates and therefore often introduce group delay dispersion on the order of multiple tens to hundreds of fs^2, this novel mirror acts as a quarter-wave plate without introducing group delay dispersion due to its reflective nature. Its capabilities are demonstrated by turning linearly polarized, few-cycle, near-octave spanning visible laser pulses into nearly circularly polarized waveforms without additional dispersion compensation.

A schematic of the operating principle is shown in Fig. 1(a). Figure 1(b) plots the polarization state of the reflected light in terms of the polarization ellipse. For perfect circular polarization, the amplitudes of the s- and p- components of the light wave are of equal amplitude and exhibit a differential phase shift of 90°. Depending on the differential phase shift, the polarization ellipse will exhibit different eccentricity. Figure 1(b) displays the simulated polarization states calculated for different differential phase shifts. The primary goal of this work is to demonstrate the development of the multilayer optical element and its implementation in laser systems.

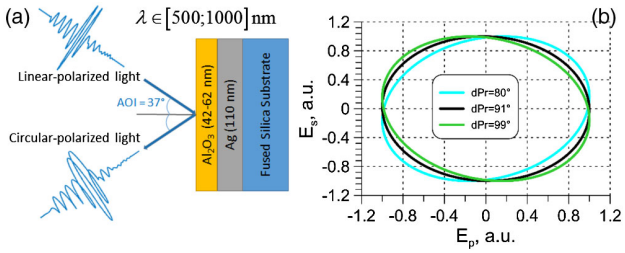

Fig. 1. (a) Operating principle of the phase-shifting optical element. (b) Polarization state diagram calculated for phase shift of 80°, 91°, and 99°.

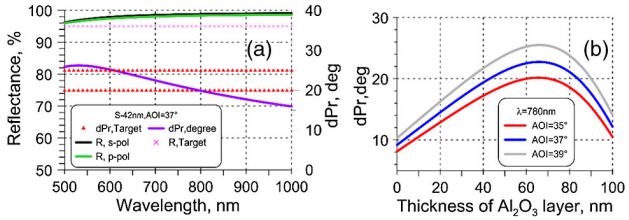

Fig. 2. (a) Reflectance and phase shift of the designed coating; triangles show the corresponding range targets. (b) Sensitivity of the differential phase shift with respect to the thickness of Al_2O_3 layer and to the AOI.

2. THEORY AND DESIGN

A metal–dielectric coating applied as quarter-wave plate requires fulfillment of the following target requirements in the broadband spectral range from 500 to 1000 nm:

- Reflectance of greater than 95% for both s- and p-polarization
- Balanced reflectance for s- and p-polarization
- A differential phase shift between the s- and p-polarization $\hat{\theta} = 90° \pm 10°$ distributed over an even number of required reflections (bounces) $N(2, 4, \text{etc})$.
- Maintenance of a high effective mirror area, with incidence angle (AOI) in the range 10°–45°
- A phase shift at the central wavelength of typical titanium: sapphire short pulse lasers $\lambda_0 = 780$ nm as close as possible to 90°

These requirements can be satisfied with the help of an $Ag - Al_2O_3$ coating containing a thick Ag layer and a thin Al_2O_3 layer.

The design process was based on minimization of the merit function MF evaluating the closeness between the target and actual spectral characteristics:

$$MF^2 = \frac{1}{L}\sum_{j=1}^{L}\Big[q\left(R^{(s)}(\mathbf{X};\lambda_j) - 95\right) + q\left(R^{(p)}(\mathbf{X};\lambda_j) - 95\right) + \left(R^{(s)}(\mathbf{X};\lambda_j) - R^{(p)}(\mathbf{X};\lambda_j)\right)^2 + 10^6\cdot\left(d\,\mathrm{Pr}\left(\mathbf{X};\lambda_j\right) - \hat{\theta}/N\right)^2\Big],$$

$$q(x) = \begin{cases} x^2, & x < 0 \\ 0, & x > 0 \end{cases}, \quad d\,\mathrm{Pr} = \varphi^{(s)} - \varphi^{(p)} \qquad (1)$$

where φ and R are actual phase of reflectance and actual reflectance, respectively; (s) and (p) correspond to the s- and p-polarization cases, respectively; $\mathbf{X} = \{d_1, \ldots, d_m\}$ is a vector of layer thicknesses; $\{\lambda_j\}$ is the wavelength grid in the spectral range 500–1000 nm; and $L = 100$. Simultaneously with minimization of the merit function [Eq. (1)], the best AOI was searched for. This is easy to do with a trial-and-error method, since angular dependencies of the spectral characteristics are quite smooth.

Multiple design attempts [16] have shown that it is not possible to achieve a phase shift of $\hat{\theta} = 90° \pm 10°$ assuming only one reflection bounce; the same occurred for the twice-smaller phase shift of 45° per bounce and two bounces. A good solution was found for four reflection bounces ($N = 4$) and a phase shift of 22.5° per bounce. A two-layer Ag/Al_2O_3 design on a fused silica substrate was chosen as the most simple and stable solution. The thickness of the silver layer was 110 nm. A solution with Al_2O_3 layer of 42 nm thickness satisfied all the requirement shown in the Introduction. Refractive index wavelength dependencies of the Al_2O_3 thin-film material and substrate were described by a well-known Cauchy formula:

$$n(\lambda) = A_0 + A_1(\lambda_0/\lambda)^2 + A_2(\lambda_0/\lambda)^4, \qquad (2)$$

where A_0, A_1, A_2 are dimensionless parameters, $\lambda_0 = 1000$ nm, and λ is specified in nanometers. The values of the Cauchy parameters of the Al_2O_3 layer and substrate were $A_0 = 1.612$, $A_1 = 5.419 \cdot 10^{-3}$, $A_2 = 1.066 \cdot 10^{-4}$ and $A_0 = 1.448$, $A_1 = 3.681 \cdot 10^{-3}$, $A_2 = -2.325 \cdot 10^{-5}$, respectively. The extinction coefficient of Al_2O_3 was specified by the exponential formula $k(\lambda) = B_0 \cdot \exp\{B_1\lambda^{-1} + B_2\lambda\}$, with $B_0 = 5984.95$, $B_1 = -1.9467$, and $B_2 = -46.556$. The optical constants of silver were initially taken from [17]. The theoretical spectral performance of the obtained design is shown in Fig. 2(a). Dependence of the phase shift on the thickness of the Al_2O_3 layer is shown in Fig. 2(b). The reflectance values for both polarizations are above 95% and quite close to each other in the full wavelength range. The differential phase shift $d\,\mathrm{Pr}(\lambda)$ in the 600–800 nm spectral range, where the most pulse energy is concentrated, lies entirely in the specified corridor from 20° to 25°. In the ranges 500–600 nm and 800–1000 nm, the $d\,\mathrm{Pr}(\lambda)$ values do not exceed 26° and 15.5°, respectively; there, spectral regions have less pulse energy. The optimal AOI was found to be 37°.

3. EXPERIMENTAL SAMPLES AND OPTICAL CHARACTERIZATION

Four identical Ag/Al_2O_3 samples, denoted S-42 nm and based on the design described in Section 2, were produced in the SyrusPro 710 high-vacuum system (BühlerLeybold Optics GmbH, Germany) by e-beam evaporation technique. The coatings were deposited on fused silica substrate of 6.35 mm thickness. The substrate temperature during the deposition was 50°. The vacuum system was pumped down to 10^{-6} mbar

before the process. The deposition rates of Ag and Al_2O_3 were 1.5 and 0.2 nm/s, respectively.

The oblique incidence reflectance for s- and p-polarization cases at AOI = 37° was measured at the Universal Reflectance Accessory of Lambda 950 (URA, Perkin Elmer) in the spectral range of 500–1100 nm; experimental reflectance values are greater than 95% in the entire spectral range. The samples were implemented into the laser setup. The details of the laser characterization are presented in Section 4.

As reflectance data does not exhibit informative features in the spectral range 400–900 nm, it does not allow one to reliably determine optical constants of silver as well as the thickness of the Al_2O_3 layer. For this reason, additional Ag/Al_2O_3 samples were produced and more informative data sets were provided as follows:

- Two samples with identical thickness of Ag (110 nm) and Al_2O_3 thicknesses of 52 and 62 nm, respectively, were produced: S-52 nm and S-62 nm.
- Transmittance and quasi-normal incidence reflectance data in the range 300–1200 nm were measured using Lambda 950 spectrophotometer and the URA, respectively.
- Ellipsometric angles Ψ and Δ in the spectral range 300–1200 nm were measured at angles of incidence of 30°, 37°, 45°, 60°, and 75° with a J.A. Woollam V-VASE ellipsometer.

A. Non-parametric Approach to Optical Characterization

In the framework of the non-parametric approach, wavelength dependencies of optical constants $n(\lambda)$, $k(\lambda)$ of the Ag films were assumed smooth functions. These dependencies, as well as the thickness of Al_2O_3 layer d, were searched for by the minimization of the discrepancy function estimating the closeness between the model $S(n, k, d; \lambda_j)$ and measured $\hat{S}(\lambda_j)$ spectral characteristics on the wavelength grid $\{\lambda_j\}$, $j = 1, \ldots, M$ in the spectral range of interest [14,22]:

$$DF^2 = \sum_{j=1}^{M} \left[\frac{S\left(n\left(\lambda_j\right), k\left(\lambda_j\right), d, \lambda_j\right) - \hat{S}\left(\lambda_j\right)}{\Delta_j} \right]^2 + \alpha_1 \sum_{j=1}^{M} \left[n''\left(\lambda_j\right)\right]^2 + \alpha_2 \sum_{j=1}^{M} \left[k''\left(\lambda_j\right)\right]^2 \rightarrow \min . \quad (3)$$

In Eq. (3), $n''(\lambda)$ and $k''(\lambda)$ denote numerical second-order derivatives of the refractive index and extinction coefficient, respectively. The second and third terms in Eq. (3) specify the additional demands on smoothness of $n(\lambda)$ and $k(\lambda)$ wavelength dependencies; the parameters α_1 and α_2 are weight factors balancing the smoothness and fitting demands. Characterization was performed using OptiLayer software [16]. The first term was considered as a sum of terms related to reflectance, transmittance, and ellipsometric measurements Ψ and Δ; Δ_j are measurement accuracies. In the course of the characterization process of S-42 nm, the thickness of Ag layer was fixed to 110 nm. Good fitting of ellipsometric and reflectance data [Figs. 3(b) and 4] by smooth wavelength dependencies $n(\lambda)$, $k(\lambda)$ were plotted in Fig. 3(a), and $d = 45.5$ nm Al_2O_3 layer thickness was achieved. At the same time, measured transmittances in the range 300–400 nm were significantly higher than the model transmittance. Then, by varying thickness of the Ag layer, a good fitting of the experimental transmittance by model transmittance was achieved for Ag thickness of 100 nm [inset in Fig. 3(b)]; varying the thickness of Ag layer did not worsen the fitting of other experimental data since they are not sensitive to the thickness of a thick metal layer on the substrate.

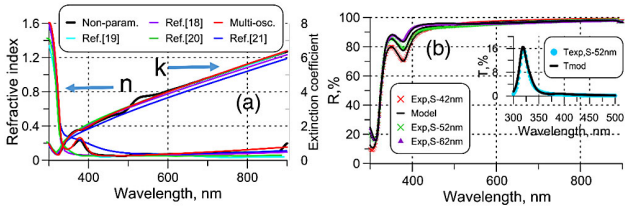

Fig. 3. (a) Comparison of the determined refractive index and extinction coefficient of Ag layer with literature data of thick films/bulk Ag [18–20] and thin film [21]. (b) Fitting of the experimental reflectance and transmittance (inset) data by model data.

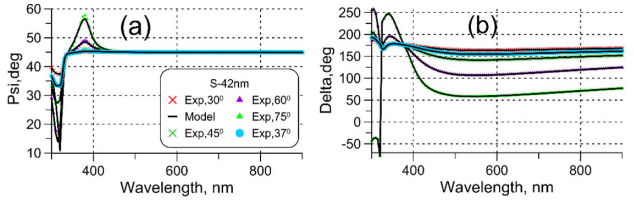

Fig. 4. Fitting of the experimental ellipsometric data by the model data related to the S-42 nm sample.

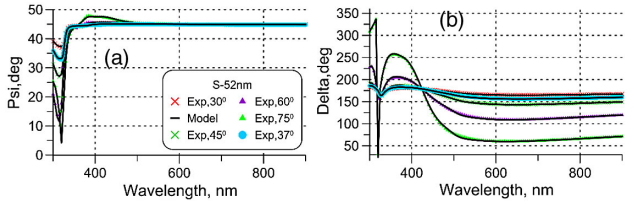

Fig. 5. Fitting of the experimental ellipsometric data by the model data related to the S-52 nm sample.

In order to verify the characterization results, measurement data related to the S-52 nm and S-62 nm samples were processed. The refractive index of Ag was fixed and the thickness of the Al_2O_3 and Ag layers was searched for. The actual thicknesses of the Al_2O_3 layers in S-52 nm and S-62 nm were found to be 56 and 72 nm, respectively; the thicknesses of Ag layers were 103 and 99 nm, respectively. The excellent fittings achieved are shown in Figs. 5 and 6.

B. Application of a Multi-oscillator Approach

Reflectance and ellipsometric spectra exhibit a pronounced dip around 320 nm that can be associated with the excitation of

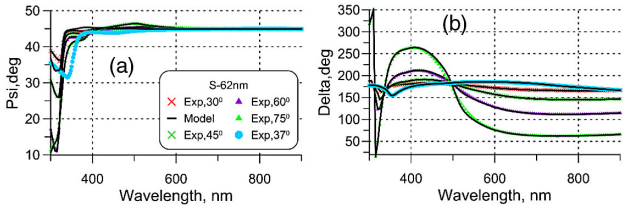

Fig. 6. Fitting of the experimental ellipsometric data by the model data related to the S-62 nm sample.

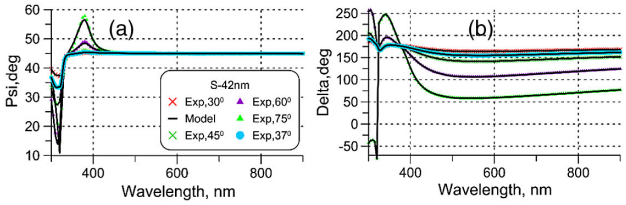

Fig. 7. Fitting of the experimental ellipsometric data by the model data related to the S-42 nm sample (multi-oscillator model).

Berreman modes, which can be excited in multilayer structures containing metal layers when the dielectric function of metal becomes close to zero [23]. Optical constants of the Ag layer were modeled using a multiple-oscillator approach as previously described [14]. In this model, the dielectric function reads as

$$\varepsilon(E) = \varepsilon_\infty - \frac{\omega_p^2}{E(E+i\gamma)} + \sum_{k=1}^{n}\left[\varepsilon_{GR,k}(E) + i\varepsilon_{GI,k}(E)\right],$$

$$\varepsilon_{GR,k}(E) = \frac{2}{\pi} p.v.\text{Cauchy}\int_0^\infty \frac{\xi\varepsilon_{GI,k}(\xi)}{\xi^2 - E^2}\mathrm{d}\xi,$$

$$\varepsilon_{GI,k}(E) = A_k\left\{\exp\left[-\left(\frac{E-E_k}{B_k}\right)^2\right] - \exp\left[-\left(\frac{E+E_k}{B_k}\right)^2\right]\right\}, \quad (4)$$

where ε_∞ is the constant polarization contribution of light–matter interaction mechanisms taking place at wavelengths below the spectral range of interest. The second term is the Drude model that accounts for the contribution of free electrons, and is described by the plasma frequency ω_p and the damping constant γ. The last term is a sum of Gaussian oscillators that can be used to account for interband electronic transitions and other possible absorption mechanisms. Each Gaussian oscillator is defined through its amplitude (A_k), central energy (E_k), and broadening (B_k); ε_{GR} and ε_{GI} denote real and imaginary parts of the Gaussian oscillators; $p.v.$ is the Cauchy principal value. An excellent fitting of the experimental ellipsometric data by model data is clearly demonstrated in Fig. 7. The obtained $n(\lambda)$ and $k(\lambda)$ wavelength dependences are in good agreement with those determined with the help of the non-parametric approach [Fig. 3(a)]. The thicknesses of Al_2O_3 layers in S-42 nm, S-52 nm, and S-62 nm were 45.5, 56.4, and 71.7 nm, respectively, quite close to the values estimated by the non-parametric approach.

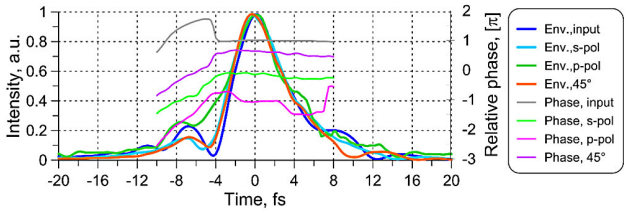

Fig. 8. Transient-grating frequency-resolved optical gating measurements of the retrieved intensity envelopes and temporal phases of the pulses along the respective polarization directions. Env. denotes intensity envelope of the pulse. See text for details.

4. INTEGRATION INTO A FEW-CYCLE LASER SYSTEM

To demonstrate the applicability of the new optics as a dispersionless quarter-wave plate for few-cycle laser pulses, four S-42 nm mirrors were integrated into a hollow-core-fiber broadened laser system producing linearly polarized sub-6 fs laser pulses [24] without additional dispersion compensation. Their orientation was chosen to realize an equal projection of the incident polarization to the s- and p-polarization directions in the mirror system, and an angle of incidence of 37°. The time structure of the linearly polarized input pulse and the polarization-converted pulse were resolved using transient-grating frequency-resolved optical gating [25] in a 20 μm thin fused silica plate (Fig. 8). To show that the polarization-converted laser pulse is short in both the s- and p-polarization directions, both directions were isolated using a reflective polarizer and individually measured. A third measurement mixing the s- and p-polarization in the 45° direction is used to ensure that both overlap in time [26]. The retrieved pulse envelopes, compared in Fig. 8, possess durations of 5.8 fs (input, intensity full width at half maximum), 6.1 fs (polarization-converted, s-pol.), 6.1 fs (polarization converted, p-pol.), and 5.8 fs (polarization converted, 45°), proving that the time structure of the input pulse is conserved by the novel reflective wave plate. The time dependences of the measured pulse phases (Fig. 8) are close to constant in the range [−4; 8] fs, where the most pulse energy is concentrated. This indicates that the Ag/Al_2O_3 optical elements do not introduce additional dispersion and phase modulation. The phase shift (95°) and group delay difference (0.3 fs) between the s- and p-polarized light fields, extracted from all three measurements using tomographic ultrafast retrieval of transverse light E-fields [26], match the values predicted by the ellipsometric measurements (Section 3) and show that the optics introduces a quarter-wave shift.

5. CONCLUSIONS AND OUTLOOK

Ag/Al_2O_3 phase-shifting mirrors were designed and produced. Careful optical characterization of the samples was performed in the spectral range 300–1200 nm based on spectral photometric

and ellipsometric measurements. Interesting spectral behavior of Ag refractive index around 320 nm was noticed. Optical constants of silver were determined using two different techniques, non-parametric and multi-oscillator, and the consistency of the results is clearly demonstrated.

The mirrors were integrated into a state-of-the-art ultrashort laser system, where they converted linearly polarized few-cycle light pulses to circular polarization. Resolving the initial and resulting pulses' time structure showed that no additional group delay dispersion compensation is necessary as for conventional waveplates. This shows that reflective waveplates employing metal–dielectric coatings can readily create circularly polarized few-cycle light fields from existing laser systems, providing a gateway to many applications in diverse fields of physics such as high-harmonics generation [27], attosecond physics [28], and the ultrafast study of 2D materials [29].

Funding. Munich-Centre for Advanced Photonics; Hrvatska Zaklada za Znanost (IP-2016–06-2168).

REFERENCES

1. M. Bass and Optical Society of America, ed., *Handbook of Optics*, 2nd ed. (McGraw-Hill, 1995).
2. H. A. Macleod, *Thin-Film Optical Filters*, 4th ed. (Taylor & Francis, 2010).
3. X.-F. Li, Y.-R. Chen, J. Miao, P. Zhou, Y.-X. Zheng, L.-Y. Chen, and Y.-P. Lee, "High solar absorption of a multilayered thin film structure," Opt. Express **15**, 1907–1912 (2007).
4. N. P. Sergeant, O. Pincon, M. Agrawal, and P. Peumans, "Design of wide-angle solar-selective absorbers using aperiodic metal-dielectric stacks," Opt. Express **17**, 22800–22812 (2009).
5. M. Zeman, R. A. C. M. M. van Swaaij, J. W. Metselaar, and R. E. I. Schropp, "Optical modeling of a-Si:H solar cells with rough interfaces: effect of back contact and interface roughness," J. Appl. Phys. **88**, 6436–6443 (2000).
6. F. Lemarquis and G. Marchand, "Analytical achromatic design of metal-dielectric absorbers," Appl. Opt. **38**, 4876–4884 (1999).
7. V. Janicki, T. V. Amotchkina, J. Sancho-Parramon, H. Zorc, M. K. Trubetskov, and A. V. Tikhonravov, "Design and production of bicolour reflecting coatings with Au metal island films," Opt. Express **19**, 25521–25527 (2011).
8. E. N. Kotlikov, E. V. Khonineva, V. N. Prokashev, and A. N. Tropin, "Spectral-splitter coatings in laser systems for the visible and infrared regions," J. Opt. Technol. **76**, 693–696 (2009).
9. A. Poddubny, I. Iorsh, P. Belov, and Y. Kivshar, "Hyperbolic metamaterials," Nat. Photonics **7**, 948–957 (2013).
10. G. Subramania, A. J. Fischer, and T. S. Luk, "Optical properties of metal-dielectric based epsilon near zero metamaterials," Appl. Phys. Lett. **101**, 241107 (2012).
11. J. Orosco and C. F. M. Coimbra, "On a causal dispersion model for the optical properties of metals," Appl. Opt. **57**, 5333–5347 (2018).
12. S. Wilbrandt and O. Stenzel, "Empirical extension to the multioscillator model: the beta-distributed oscillator model," Appl. Opt. **56**, 9892–9899 (2017).
13. T. V. Amotchkina, V. Janicki, J. Sancho-Parramon, A. V. Tikhonravov, M. K. Trubetskov, and H. Zorc, "General approach to reliable characterization of thin metal films," Appl. Opt. **50**, 1453–1464 (2011).
14. T. V. Amotchkina, M. K. Trubetskov, A. V. Tikhonravov, V. Janicki, J. Sancho-Parramon, and H. Zorc, "Comparison of two techniques for reliable characterization of thin metal-dielectric films," Appl. Opt. **50**, 6189–6197 (2011).
15. H. Höchst, R. Patel, and F. Middleton, "Multiple-reflection phase shifter: a viable alternative to generate circular-polarized synchrotron radiation," Nucl. Instrum. Methods Phys. Res., Sect. A **347**, 107–114 (1994).
16. A. V. Tikhonravov and M. K. Trubetskov, "OptiLayer software," http://www.optilayer.com.
17. E. Palik, *Handbook of Optical Constants of Solids II* (Academic, 1991).
18. H. U. Yang, J. D'Archangel, M. L. Sundheimer, E. Tucker, G. D. Boreman, and M. B. Raschke, "Optical dielectric function of silver," Phys. Rev. B **91**, 235137 (2015).
19. P. B. Johnson and R. W. Christy, "Optical constants of the noble metals," Phys. Rev. B **6**, 4370–4379 (1972).
20. S. Babar and J. H. Weaver, "Optical constants of Cu, Ag, and Au revisited," Appl. Opt. **54**, 477–481 (2015).
21. A. Ciesielski, L. Skowronski, M. Trzcinski, and T. Szoplik, "Controlling the optical parameters of self-assembled silver films with wetting layers and annealing," Appl. Surf. Sci. **421**, 349–356 (2017).
22. O. Stenzel and R. Petrich, "Flexible construction of error functions and their minimization: application to the calculation of optical constants of absorbing or scattering thin-film materials from spectrophotometric data," J. Phys. D **28**, 978–989 (1995).
23. W. D. Newman, C. L. Cortes, J. Atkinson, S. Pramanik, R. G. DeCorby, and Z. Jacob, "Ferrell-Berreman modes in plasmonic epsilon-near-zero media," ACS Photon. **2**, 2–7 (2015).
24. W. Schweinberger, A. Sommer, E. Bothschafter, J. Li, F. Krausz, R. Kienberger, and M. Schultze, "Waveform-controlled near-single-cycle milli-joule laser pulses generate sub-10 nm extreme ultraviolet continua," Opt. Lett. **37**, 3573–3575 (2012).
25. J. N. Sweetser, D. N. Fittinghoff, and R. Trebino, "Transient-grating frequency-resolved optical gating," Opt. Lett. **22**, 519–521 (1997).
26. P. Schlup and R. A. Bartels, "Impact of measurement noise in tomographic ultrafast retrieval of transverse light E-fields (TURTLE) ultrashort polarization characterization," IEEE Photon. J. **1**, 163–171 (2009).
27. A. Fleischer, O. Kfir, T. Diskin, P. Sidorenko, and O. Cohen, "Spin angular momentum and tunable polarization in high-harmonic generation," Nat. Photonics **8**, 543–549 (2014).
28. P. Eckle, M. Smolarski, P. Schlup, J. Biegert, A. Staudte, M. Schöffler, H. G. Muller, R. Dörner, and U. Keller, "Attosecond angular streaking," Nat. Phys. **4**, 565–570 (2008).
29. H. K. Kelardeh, V. Apalkov, and M. I. Stockman, "Attosecond strong-field interferometry in graphene: chirality, singularity, and Berry phase," Phys. Rev. B **93**, 155434 (2016).